CsI Calorimeter for KOTO experiment

Kazufumi Sato[*†]
Department of Physics, Osaka University
E-mail: sato@champ.hep.sci.osaka-u.ac.jp

The J-PARC KOTO experiment searches for $K_L \to \pi^0 \nu \bar{\nu}$ decay by observing two photons from π^0 using a CsI calorimeter. The performance of the CsI calorimeter was measured in a beam test held in 2012. We have measured that the energy resolution is $\sigma_E/E = 1.9\%/\sqrt{E[GeV]}$ and the position resolution is $\sigma_X[mm] = 1.8 \oplus 2.8/\sqrt{E[GeV]} \oplus 1.73/E[GeV]$. One of the features of the KOTO CsI calorimeter is an ability to record electromagnetic shower shape. The shower shape information is effective to suppress the background events caused by overlapping showers, and photons with large incident angles. Based on the Monte Calro studies, we can reject 90% (94%) of the former (latter) background events while keeping 85% (90%) of signal events using the shower shape information.

Calorimetry for High Energy Frontiers - CHEF 2013,
April 22-25, 2013
Paris, France

[*]Speaker.
[†]for the KOTO collaboration

1. KOTO experiment

The J-PARC KOTO experiment [1] searches for the $K_L \to \pi^0 \nu\bar{\nu}$ decay. The branching ratio of this decay is related to the imaginary part of the CKM matrix elements, and it can be calculated with a small uncertainty ($\simeq 2.5\%$) in the standard model. Any difference from the standard model expectation suggests the evidence of new physics. This decay is not observed yet because the branching ratio is expected to be very small, at the order of 10^{-11}. The current upper limit is 2.6×10^{-8} at 90% confidence level, which was given by the KEK E391A experiment [2]. The KOTO experiment will make the first observation of the $K_L \to \pi^0 \nu\bar{\nu}$ decay using a high intensity K_L beam at J-PARC.

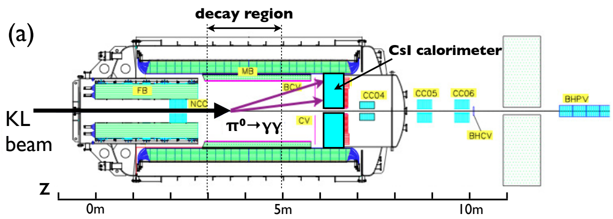

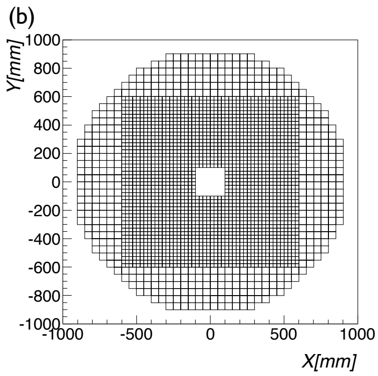

Figure 1: (a) Layout of the KOTO Detector. (b) Layout of the KOTO CsI calorimeter.

The $K_L \to \pi^0 \nu\bar{\nu}$ decay has a unique feature that observable particles are nothing but two photons from π^0, and the π^0 has a finite transverse momentum (p_{T}) due to neutrinos. KOTO looks for this unique final state using a barrel-shaped detector shown in Fig.1(a). The energies and incident positions of the two photons are measured with a CsI calorimeter located downstream part of the barrel. The p_{T} and z vertex position of the mother π^0 is calculated from these kinematics with two assumptions: 1) the decay vertex is located on the beam axis, and 2) the invariant mass of the two photons should be equal to the mass of π^0. To make sure that there are no other observable particle, the decay region is surrounded by veto counters.

2. KOTO CsI calorimeter

The layout of the CsI calorimeter is shown in Fig.1(b). It consists of 2716 undoped CsI crystals which were used in the FNAL KTeV experiment [3]. Each crystal is 50 cm long (27 radiation lengths). This reduces the amount of shower leakage from the rear to be less than 0.5% and improves the energy resolution. The cross section of the crystals in the inner region is 2.5×2.5 cm^2, while that in the outer region is 5.0×5.0 cm^2. Because the Moliere radius of CsI is 3.57 cm, an electromagnetic shower spreads over many crystals. It enables us to obtain the information of shower shape, which is useful to suppress some background events, as explained in details later. Waveforms from each crystal are recorded by 125-MHz FADC.

3. Calorimeter Performance

The performance of the CsI calorimeter directly affects the quality of the KOTO experiment because it is the sole detector to measure the kinematic information of both signal and background events. It is thus important to understand its energy and position resolutions. In February and June of 2012, we conducted tests to measure the resolutions using the K_L beam at J-PARC. We used electrons from $K_L \to \pi e \nu$ decays. Energies and positions of electrons, which were measured with the CsI calorimeter, were compared with those measured by a referential spectrometer which consisted of 0.7-T magnet and three drift chambers and was located in front of the calorimeter. The layout of the beam test is shown in Fig.2. At that time, veto counters were not installed yet.

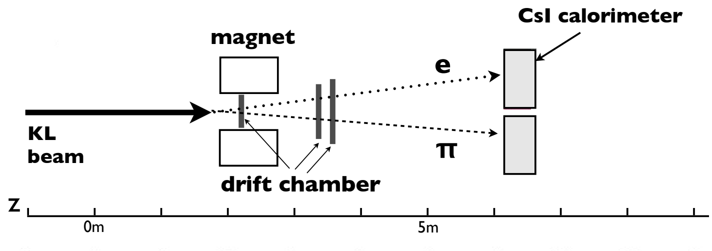

Figure 2: Schematic view of the CsI peaformance test which was conducted in 2012.

3.1 Energy Resolution

Figure 3 shows the distribution of the ratio of the calorimeter energy over the spectrometer momentum, E/p. The width of the E/p distribution was estimated by fitting the peak with Gaussian, and represented as a function of momentum in Fig.4(a). The contribution of the spectrometer resolution and the fluctuation due to materials in front of the calorimeter are also shown in the figure. Subtracting these contributions, the energy resolution of the CsI calorimeter is estimated to be:

$$\frac{\sigma}{E} = \frac{1.9\%}{\sqrt{E[GeV]}}, \tag{3.1}$$

as shown in Fig.4(b).

3.2 Position Resolution

The electron incident position, which was reconstructed by the CsI calorimeter, was compared with the position tracked by the spectrometer in order to derive the position resolution. The width of the distribution of the difference between these two positions, ΔX, was evaluated by fitting with a Gaussian, and represented as a function of momentum as shown in Fig.5(a). Subtracting the contribution of the spectrometer resolution and the materials, we estimated the position resolution of the CsI calorimeter to be:

$$\Delta X[mm] = 1.8 \oplus 2.8/\sqrt{E[GeV]} \oplus 1.73/E[GeV], \tag{3.2}$$

as shown in Fig.5(b).

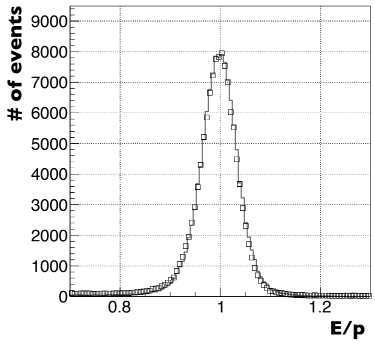

Figure 3: E/p distribution for electrons from $K_L \to \pi e \nu$ decay. The white squares show the data, and the histogram shows the expectation from Monte Calro simulations.

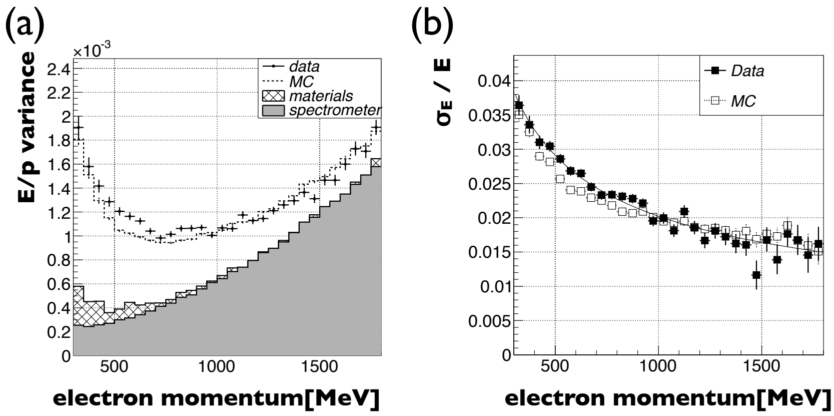

Figure 4: (*a*) Momentum dependence of the variance of the E/p distribution. The dots with error bars show the data and the dotted-line histogram shows the expectation from Monte Calro simulations. The contribution of the resolution of the spectrometer (gray-filled histogram) and the fluctuation due to materials (meshed histogram) are also shown. (*b*) Momentum dependence of $\sigma(E)/E$. The black squares shows the data while the white squares shows the expectation from Monte Calro simulations.

4. Shower shape information

The KOTO CsI calorimeter has a capability to record shower shapes. There are two applications of shower shape information. In this section, I will describe their performances based on the Monte Calro studies .

4.1 Suppression for the fusion background

One of the main sources of background is called "fusion" events. It arises from the $K_L \to \pi^0\pi^0$ decay. If two of four photons from two π^0s hit the calorimeter close to each other, their showers will overlap and look like one photon, as shown in Fig.6. This event is not easy to suppress because this event has only one extra photon to veto and has similar kinematics as $K_L \to \pi^0 \nu \bar{\nu}$. However, a fused shower should have an unusual shape. To quantify this shape information, we compare the

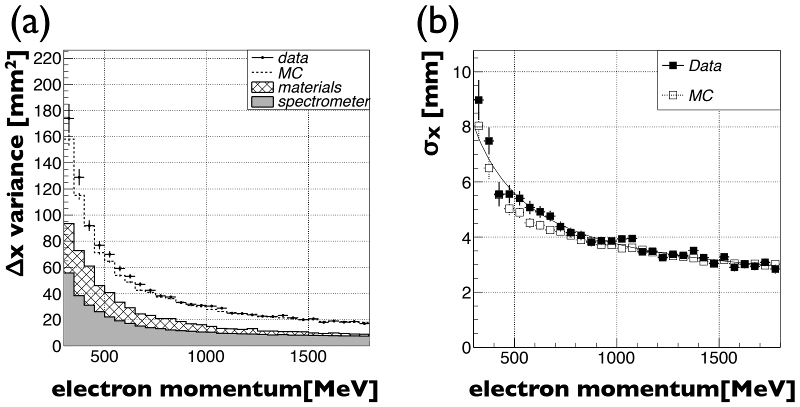

Figure 5: (*a*) Momentum dependence of the variance of ΔX. The dots with error bars show the data, and the dotted-line histogram shows the expectation from Monte Calro simulations. The contribution of the resolution of the spectrometer (gray-filled histogram) and the fluctuation due to materials (meshed histogram) are also shown. (*b*) Momentum dependence of σ_X. The black squares show the data, while the white squares shows the expectation from Monte Calro simulations.

observed shower shape with a reference shape derived from Monte Calro studies. For the reference shape, the expected energy deposit and its RMS for each crystal around the photon incident position were recorded. We defined the χ^2 value as:

$$\chi^2 = \sum_i \left(\frac{E_i^{obs} - E_i^{ref}}{\sigma_i^{ref}} \right)^2 , \tag{4.1}$$

where $E^{obs(ref)}$ denotes observed (expected) energy deposit in each crystal, and σ^{ref} is the RMS of the expected energy deposit. Summation is done for crystals whose energy deposit is more than 3 MeV. A reference shape is prepared for various photon energies, polar angles and azimuthal angles. The most suitable reference is selected event by event to calculate χ^2. Figure 7(a) shows the χ^2 distribution of the $K_L \to \pi^0 \nu \bar{\nu}$ events and the fusion background events. Fusion events tend to have large χ^2 values. Imposing a cut on this value, we can reject 90% of fusion background events with an 85% signal acceptance (Fig.7(b)).

4.2 Suppression for η background

As explained in Section 1, we assume that the observed two photons are from π^0 when reconstructing the vertex, but we are unable to tell whether those photons are actually from π^0 or not. This ambiguity raises another type of background called the η background. Consider the case in which a beam neutron interacts with materials and generates η decaying to two photons (Fig.8). In this case, the reconstructed vertex assuming π^0 is located more upstream than the vertex assuming η. Consequently, the incident angles of the photons, which are calculated from the vertex position, are different between these two assumptions. In order to reject this η background, we developed an angle discrimination method using the shower shape. We prepared a two-dimensional probability density function (PDF) of crystal X(Y) positions and the energy deposits projected to the X(Y)

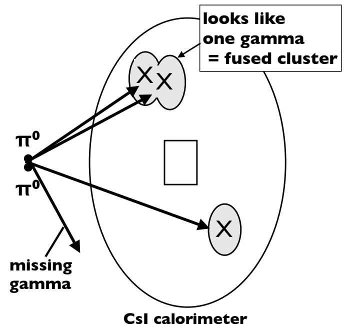

Figure 6: Schematic view of fusion background.

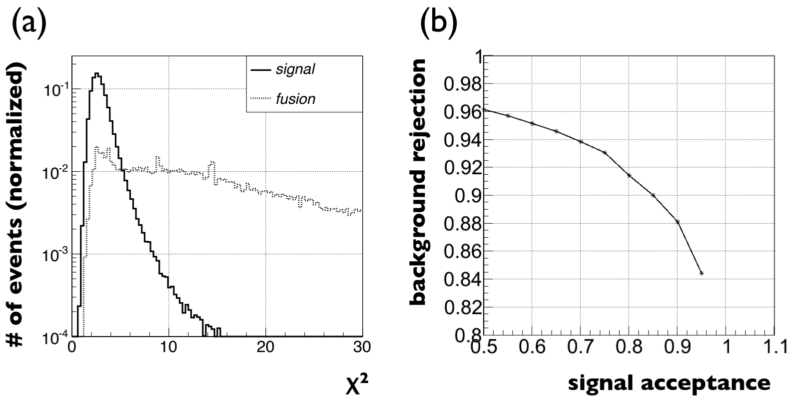

Figure 7: (*a*) Shape χ^2 distribution. The solid line is for the $K_L \to \pi^0 \nu\bar{\nu}$ events and the dotted line is for the fusion events. (*b*) Background rejection vs signal acceptance.

axis. The PDF shape depends on the incident angle of the photon as shown in Fig.9. The PDF is prepared for various incident angles, azimuthal angles and energies. We calculate likelihoods using these PDF for the two assumptions: π^0 and η. The ratio of the two likelihoods, $L_{\pi^0}/(L_{\pi^0}+L_\eta)$, has a good discrimination power, as shown in Fig.10(a). Cutting on this value, we can reject 94% of η background events with a 90% signal acceptance (Fig.10(b)).

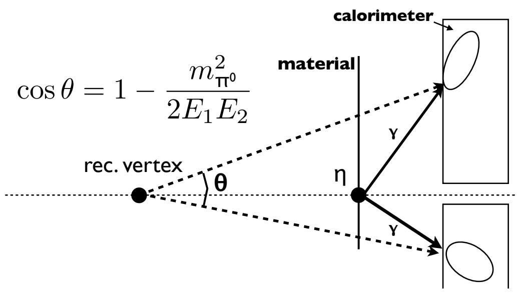

Figure 8: Schematic view of η background.

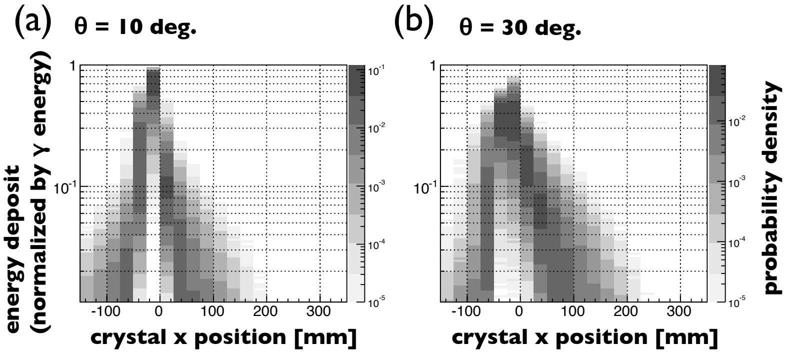

Figure 9: Two-dimensional probability density function for (*a*) $\theta = 10$deg and (*b*) for $\theta = 30$deg. The photon energy is 450MeV and the azimuthal angle is 0 degree.

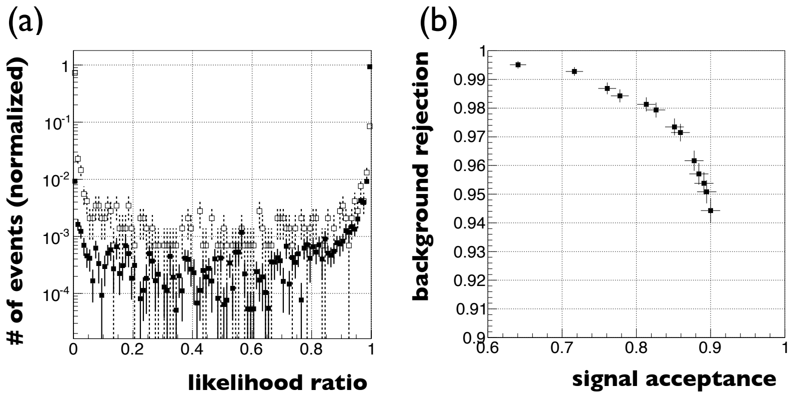

Figure 10: (*a*) Likelihood ratio distribution. The black squares are for the $K_L \to \pi^0 \nu \bar{\nu}$ events and the white squares are for the η events. (*b*) η background rejection vs signal acceptance.

5. Conclusion

The CsI calorimeter is most important in the KOTO detector. A beam test was conducted to measure its energy and position resolutions in 2012. The energy resolution was $\sigma_E/E = 1.9\%/\sqrt{E[GeV]}$ and the position resolution was $\sigma_X[mm] = 1.8 \oplus 2.8/\sqrt{E[GeV]} \oplus 1.73/E[GeV]$. Based on the Monte Calro studies, we can reject 90% (94%) of fusion (η) background events while keeping 85% (90%) of signal events using shower shape information.

References

[1] J. Comfort *et al.* Proposal for $K_L^0 \to \pi^0 \nu \bar{\nu}$ Experiment at J-PARC. *http://j-parc.jp/researcher/Hadron/en/Proposal_e.html*, 2006.

[2] J.K. Ahn *et al.* Experimental study of the decay $K_L^0 \to \pi^0 \nu \bar{\nu}$. *Phys. Rev. D*, **81**:072004, 2010.

[3] E. Cheu *et al.* Proposal to Continue the Study of Direct CP Violation and Rare Decay Processes in KTeV in 1999. *http://ktev.fnal.gov/public/*, 1997.